Computational Materials Science 167 (2019) 13–18

Contents lists available at ScienceDirect

Computational Materials Science

journal homepage: www.elsevier.com/locate/commatsci

Characterization of two-dimensional $Ga_{1-x}Al_xN$ ordered alloys with varying chemical composition

M. Kanli[a], A. Onen[a], A. Mogulkoc[b], E. Durgun[a,*]

[a] UNAM – National Nanotechnology Research Center and Institute of Materials Science and Nanotechnology, Bilkent University, Ankara 06800, Turkey
[b] Department of Physics, Faculty of Sciences, Ankara University, Ankara 06100, Turkey

ARTICLE INFO

Keywords:
2D materials
III-nitrides
Alloys
Ab initio
DFT

ABSTRACT

Similar to bulk semiconductors, alloying suggests a promising strategy to tailor the fundamental properties of two-dimensional (2D) systems with constituent composition. In that sense, detailed understanding of atomic structure and stability analysis are required to predict and design new 2D alloys. In this paper, we analyze the structural, mechanical, electronic, thermal, and optical properties of monolayer $Ga_{1-x}Al_xN$ ordered alloys for varying concentration by using *ab initio* methods. Following the determination of ground state geometries by taking into account the possibility of segregation, we investigate the stability of the considered structures by phonon spectrum analysis and high temperature molecular dynamics calculations. Our results indicate that the properties of 2D $Ga_{1-x}Al_xN$ can be modified continuously by controlling the Al concentration. Tunability of the desired properties broadens the possible usage of 2D semiconductors in nanoscale applications.

1. Introduction

Intensive research on the family of group III-nitrides (or group III-N) [1,2] with tunable band gap that spans from the infrared to the deep ultraviolet, has led to diverse optoelectronic devices involving light emitting diodes, detectors, and lasers [3–5]. Following their theoretical prediction [6–8], the realization of two-dimensional (2D) GaN [9] and AlN [10,11] has expanded the promising applications of group III-N semiconductors to low-dimensional systems and also makes miniaturization of the current devices probable. The free-standing monolayers of GaN and AlN can have different forms [12], but in general their graphene-like planar honeycomb structures, namely h-GaN [13] and h-AlN [14] have been rigorously examined. Both h-GaN and h-AlN are wide band gap semiconductors with exceptional properties which have been revealed in extensive studies [12]. For instance, their 2D sheets, decorated with H or F atoms have been explored and their ferromagnetic and half-metallic characteristics have been pointed out [15]. The tunable electronic properties of 2D group III-nitride heterostructures have been investigated and their potential applications including solar cells have been suggested [16–20]. Chemical functionalization of GaN [21] and AlN [22] monolayers with various adatoms have been shown to provide novel electronic and magnetic properties.

The applications of 2D semiconductors, in specific group III-nitrides are limited by scalability and/or formability issues, and also controllable modification of their (opto-) electronic properties [8]. Alloying offers a promising strategy, since band gap of bulk semiconductors can be directly controlled with constituent composition [23–25]. Even though alloying in 2D is different from bulk systems due to dimensionality effects and boundary conditions [16,26,27], this approach is recently realized for 2D transition metal dichalcogenide (TMD) alloys and $Mo_{1-x}W_xS_2$[17], $Mo_{1-x}W_xSe_2$[28,29], and $MoS_{2(x)}Se_{2(1-x)}$[30] have been synthesized within this class. These systems have been analyzed in detail and their tunable optical properties have been demonstrated [17,31]. In addition to TMDs, hexagonal boron-carbon-nitride (h-BC_xN) composites have been examined by scanning tunneling microscopy to reveal the dynamics of mixing and order-disorder transitions which are crucial for growth of 2D alloys [32]. The alloys of 2D group IV systems ($Si_{1-x}C_x$, $Si_{1-x}Ge_x$, and $Ge_{1-x}C_x$) have been studied and the variation of their thermodynamic, structural, and electronic properties with composition have been explored [33]. The geometry and band structures of 2D SbBi alloy films have been studied by *ab initio* methods and their topological properties including topological phase transitions have been examined [34]. Among group III-nitrides, the fundamental properties of $In_xGa_{1-x}N$ alloys have been explored by first-principles calculations, and structural parameters, mixing enthalpies, and band gaps for different structures have been reported. Although bulk $Ga_{1-x}Al_xN$ have been synthesized [35,36] and studied extensively [37], apart from studies on doping of

* Corresponding author.
E-mail address: durgun@unam.bilkent.edu.tr (E. Durgun).

https://doi.org/10.1016/j.commatsci.2019.05.018
Received 18 January 2019; Received in revised form 8 May 2019; Accepted 9 May 2019
Available online 18 May 2019
0927-0256/

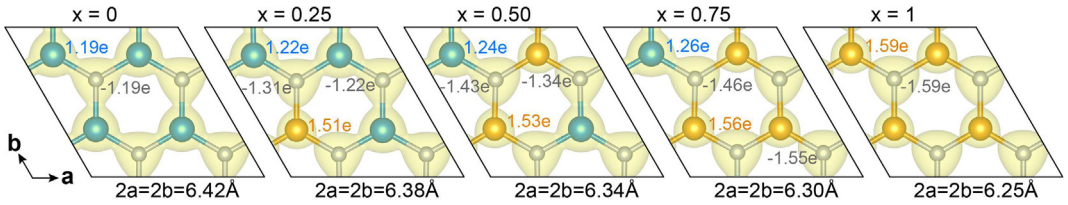

Fig. 1. Top views of the optimized atomic structures of $Ga_{1-x}Al_xN$ alloys with bond charges. The 2 × 2 super cell (with respect to primitive unit cell of pristine system) are laid out by solid lines as 2D parallelogram. Turquoise, yellow, grey spheres stand for Ga, Al and N atoms, respectively. Lattice constants (a, b) and charge transfer are indicated for each system.

2D GaN with Al [38], alloys of GaN and AlN are not yet considered albeit their structural similarity and lattice match and also possibility of using them in various optoelectronic applications [27,17].

Motivated with the recent synthesis of 2D GaN and AlN, and their potential implementation in nanoelectronics, we examine the fundamental properties of $Ga_{1-x}Al_xN$ ordered alloys [39,40] in planar and hexagonal form, where x indicates the Al content. Starting from the pristine h-GaN and h-AlN which also set the end-points, optimized structures of alloys are obtained and cohesive/substitution energies are calculated. Following the analysis on phase segregation, the dynamic stability of the alloys is taken into account and is studied by phonon spectrum analysis and high temperature molecular dynamics (MD) simulations. Next, the variation of structural, mechanical, electronic, thermal, and optical properties of $Ga_{1-x}Al_xN$ alloys ($0 < x < 1$, 0.25 interval) are explored and trends are revealed.

2. Method

We performed first principles calculations using the Vienna Ab initio Simulation Package (VASP) [41–44] based on density functional theory (DFT). Projector-augmented wave (PAW) potentials [45,46] were used to describe Ga, Al, and N elements and plane-wave basis set with an energy cutoff of 520 eV was taken. The exchange-correlation functional was approximated by generalized gradient approximation (GGA) within Perdew, Burke, and Ernzerhof (PBE) scheme [47]. The Brillouin zone of 2 × 2 super cell was sampled with 21 × 21 × 1 **k**-point mesh set by Monkhorst-Pack method [48]. The atomic positions were optimized by using conjugate gradient method following the minimization of the total energy of the system. The energy and force convergence criteria between the two consecutive steps were taken to be 10^{-5} eV and 0.01 eV/Å, respectively. A super cell with a vacuum spacing of ~20 Å was used to avoid spurious interaction between periodic images in adjacent cells. The density derived electrostatic and chemical (DDEC) approach method was utilized for the analysis of interionic charge-transfer [49].

Following expressions are used for; cohesive energy,

$$E_c(x) = (1-x)E_T(\mathrm{Ga}) + xE_T(\mathrm{Al}) + E_T(\mathrm{N}) - E_T(\mathrm{Ga}_{1-x}\mathrm{Al}_x\mathrm{N}) \quad (1)$$

average substitution energy,

$$E_{sub}(x) = ([xE_T(\mathrm{Al}) + E_T(\mathrm{GaN})] - [(xE_T(\mathrm{Ga}) + E_T(\mathrm{Ga}_{1-x}\mathrm{Al}_x\mathrm{N})])/x \quad (2)$$

free energy of mixing,

$$F_{mix}(x) = E_{mix}(x) - TS_{mix}(x) \quad (3)$$

and internal energy of mixing,

$$E_{mix}(x) = E_T(\mathrm{Ga}_{1-x}\mathrm{Al}_x\mathrm{N}) - (1-x)E_T(\mathrm{GaN}) - xE_T(\mathrm{AlN}) \quad (4)$$

where E_T(Ga), E_T(Al), E_T(N), E_T(GaN), E_T(AlN), and $E_T(Ga_{1-x}Al_xN)$ correspond to total energy of single Ga, single Al, single N, h-GaN, h-AlN, and $Ga_{1-x}Al_xN$ alloy. S and T indicate entropy and temperature, respectively. All energies are normalized to unit cell of pristine systems.

As fundamental band gaps are underestimated at GGA level, we also performed calculations with hybrid functionals (HSE06) [50,51], which is formed by mixing 25% of the Fock exchange with 75% of the PBE exchange and 100% of the PBE correlation energy.

Phonon spectra of $Ga_{1-x}Al_xN$ were calculated by Phonopy package [52] based on Density Functional Perturbation Theory (DFPT) implemented in VASP. The dynamical stability of the structures was further tested by *ab initio* molecular dynamics (MD) calculations using microcanonical ensemble by scaling the atomic velocities at 300 K, 600 K, and 900 K for 3 ps total simulation time. A larger super cell (6 × 6 × 1) was used for the stability analysis.

The frequency dependent dielectric functions of the structures were calculated by using random phase approximation (RPA) within GGA-PBE with an increased **k**-point mesh of 117 × 117 × 1 and including a total number of 96 bands.

3. Results and discussion

3.1. Structural properties and energetics

We start from the pristine h-GaN and h-AlN systems, monolayers of which have stable, planar honeycomb structures with calculated lattice constants, a of 3.21 Å and 3.13 Å, respectively [12,7,13,14]. Following the optimization of pristine structures, we design $Ga_{1-x}Al_xN$ ordered alloys[39,40] for x = 0, 0.25, 0.50, 0.75, 1 where x refers to Al content. 2 × 2 super cell (with respect to primitive unit cell of bare systems) which is shown in Fig. 1 is considered. $Ga_{1-x}Al_xN$ has hexagonal lattice similar to pristine systems and optimized lattice constant, a decreases with increasing x following Vegard's Law [53,54] as illustrated in Fig. 2(a). Buckled geometries are also tested, however the planarity is preserved for all x values. Hybridization among sp^2 orbitals of cation (Ga or Al) and anion (N) form strong σ-bonds and perpendicular p_z orbitals form π-bonds which maintain the planar geometry. As expected there is a charge transfer (Q^*) from cation to anion atoms which is shown in Fig. 1 where positive (negative) values indicate charge donation (accumulation). The charge transferred to N gradually increases with increasing x which is correlated with the electronegativity difference between Al and Ga. Similar to a, the cohesive energy (E_c) of the alloy varies almost linearly with x and it increases with increasing Al content as presented in Fig. 2(b). Owing to similar geometry and lattice match, 2 × 2 super cell is tested to be sufficient to study the fundamental properties of the ordered patterns [55]. When calculations are repeated with 4×4 super cell with different arrangements of Al at specified x, same a values are obtained and E_c differs only up to ±10 meV.

One of the possible methods to manufacture such alloys is the chemical vapor deposition (CVD) technique and in that sense the energy required to substitute Ga with Al (E_{sub}) gives an indication about feasibility of the procedure. As shown in Fig. 2(c), the calculated average E_{sub} is positive for all x, implying that substitution is energetically favored. This result is correlated with the E_c of end-point pristine systems where E_c(AlN) is significantly larger than E_c(GaN). We also calculate step-wise E_{sub} in addition to average E_{sub} formulated in the Methodology part. For this case, the energy of consecutive systems are compared instead of only bare h-GaN and similar results are obtained. Even though E_{sub} is positive, it does not guarantee that

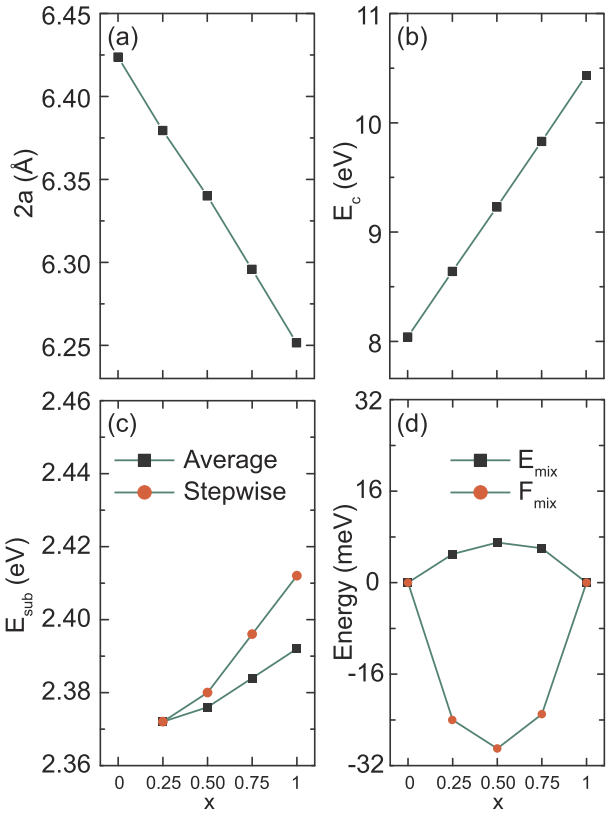

Fig. 2. The variation of (a) Lattice constant, a (b) Cohesive energy, E_c (c) Substitution energy, E_{sub}), and (d) Mixing energy, E_{mix} with x.

substitution is spontaneous. In order to analyze the reaction path for substitution, we perform Nudged Elastic Band (NEB) calculations [56], starting from adsorption cite of Al on h-GaN. Our calculations indicate that there is a small energy barrier (79 meV) for Al to substitute Ga. The details of NEB calculation are available as Supplemental material[57]. These results indicate the possibility of forming $Ga_{1-x}Al_xN$ by substitution of Ga with Al atoms.

Finally, we calculate the free (F_{mix}) and internal energy of mixing (E_{mix}) for $Ga_{1-x}Al_xN$. Even $E_{mix}(x)$ is small but positive (up to 6 meV/cell), F_{mix} becomes negative once mixing entropy is taken into account as illustrated in Fig. 2(d). The entropic contributions promote mixing and the suggested alloys are thermodynamically stable without tendency of segregation at ambient temperatures. All the obtained results are summarized in Table 1.

3.2. Stability

Although negative F_{mix} at ambient temperature points out that alloy is energetically favored over segregated phases, we also analyze the dynamic stability of $Ga_{1-x}Al_xN$ systems. Firstly, we calculate the phonon frequency spectrum for all x. As shown in Fig. 3, all the phonon frequencies are positive, indicating that there are no imaginary modes in the spectrum and thus demonstrates the stability of the considered structures. Additionally, gradual shift of optical modes with increasing x is noticed which can be correlated with the reduced total atomic mass and stronger bonds. To further test the stability against thermal excitation, we perform *abinitio* MD calculations on prototype $Ga_{0.5}Al_{0.5}N$ system. We start from 300 K and gradually increase the temperature to 600 K and finally 900 K for total simulation time of 3 ps. Apart from small fluctuations, the structure remains stable even at 900 K indicating a dynamic stability. The snapshots of the atomic structure at different temperatures are given as Supplemental material[57].

3.3. Mechanical properties

Resolving the atomic structure and stability, we analyze the fundamental properties starting from the mechanical response in the elastic regime. Strain engineering is a commonly used strategy to modify the physical properties of 2D systems [58,59]. We calculate the in-plane stiffness (Y_{2D}) and Poisson's ratio (ν) of considered systems by using the following formulas:

$$Y_{2D} = \frac{c_{11}^2 - c_{12}^2}{c_{11}} \quad \text{and} \quad \nu = \frac{c_{12}}{c_{11}} \tag{5}$$

where c_{ij}'s are the elastic constants (hydrostatic and shear terms).

The obtained values which are also listed in Table 1 for pristine h-GaN (Y_{2D} = 110 N/m; ν = 0.43) and h-AlN (Y_{2D} = 114 N/m; ν = 0.46) are in agreement with previous studies [12]. Both Y_{2D} and ν slightly escalates with increasing x as the endpoint values are close to each other and linear variation is not explicit [60] as shown in Fig. 4(a) and (b). When compared, Y_{2D} of $Ga_{1-x}Al_xN$ is significantly smaller than that of h-BN [61] (289 ± 24 N/m) which is another member of 2D group III-nitrides, because of weakened Ga(Al)–N bond with respect to B–N bond (*i. e* $Ga_{1-x}Al_xN_1$ is softer). On the other hand ν is almost double times that of h-BN and also significantly larger than most of the realized 2D systems [59].

3.4. Electronic properties

Similar to their pristine constituents, $Ga_{1-x}Al_xN$ alloys are non-magnetic, wide band gap semiconductors as shown in Fig. 5. The (in-direct) fundamental band gap (E_{g-i}) arises from $\pi - \pi^*$-bands derived from antibonding-π and bonding-π-bonds separated by a significant energy. The conduction band minimum (CBM) shifts to higher energy levels with increasing Al content, resulting in widening of E_{g-i}. This widening of E_{g-i} with x can be attributed the common-anion rule which anticipates an increase in band gap with decreasing atomic number, which in general holds for isovalent, common-cation (or anion) bulk semiconductors. Different from their bulk counterparts, $Ga_{1-x}Al_xN$ have indirect band gap between Γ-K points, ranging from 2.15 eV to 2.91 eV (calculated at DFT-PBE level) set by pristine systems. As expected, E_{g-i} blue-shifts once HSE06 correction is applied but the band profile and trends remained the same (Fig. 6). The dependence of E_{g-i} on x is nonlinear and deviates from Vegard's Law. The deviation from linearity can be quantified by a bowing parameter (β) which can be

Table 1
Optimized lattice constant a, bond length between cation and anion d_{Ga-N} and d_{Al-N}, cohesive energy E_c, average substitution energy E_{sub}, Poisson's ratio ν, in-plane stiffness Y_{2D}, charge transfer from cation to anion Q^*, indirect band gap E_{g-i} (HSE06 results are given in parenthesis) of $Ga_{1-x}Al_xN$ alloy.

	a (Å)	d_{Ga-N} (Å)	d_{Al-N} (Å)	E_c (eV/pair)	E_{sub} (eV)	ν –	Y_{2D} (N/m)	Q^* (e^-)	E_{g-i} (eV)
GaN	3.21	1.854	–	8.04	–	0.43	110	1.19	2.15 (3.42)
$Ga_{0.75}Al_{0.25}N$	3.19	1.853	1.807	8.64	2.371	0.44	110	1.32	2.41 (3.65)
$Ga_{0.50}Al_{0.50}N$	3.17	1.855	1.806	9.23	2.376	0.44	112	1.39	2.62 (3.81)
$Ga_{0.25}Al_{0.75}N$	3.15	1.853	1.807	9.83	2.382	0.45	112	1.46	2.78 (3.95)
AlN	3.13	–	1.805	10.43	2.390	0.46	114	1.59	2.91 (4.04)

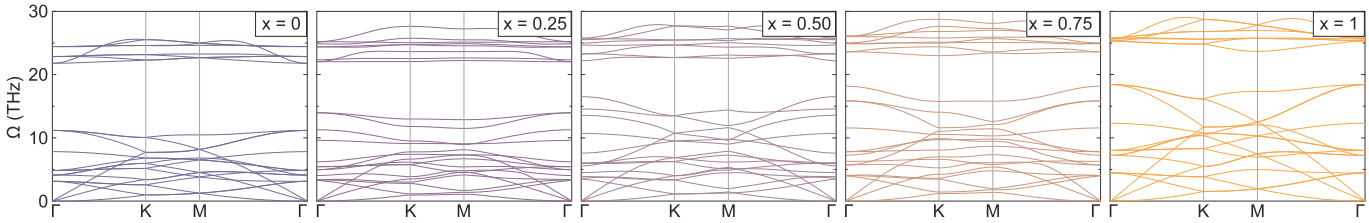

Fig. 3. Phonon dispersion bands along major symmetry directions in the Brillouin zone calculated for $Ga_{1-x}Al_xN$ alloys. The 2×2 super cell (with respect to primitive unit cell of pristine system) is considered.

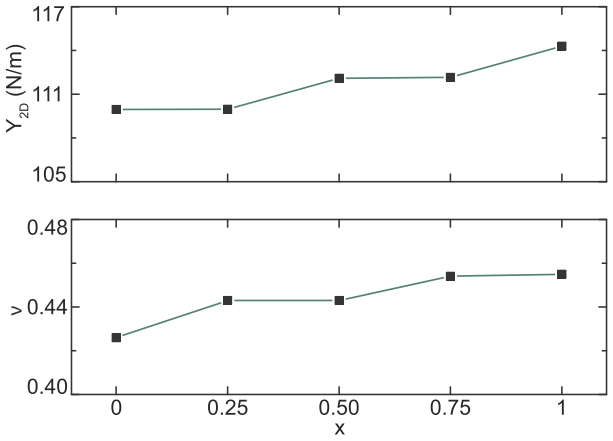

Fig. 4. The variation of (a) in-plane stiffness (Y_{2D}) and (b) Poisson's ratio (ν) with x.

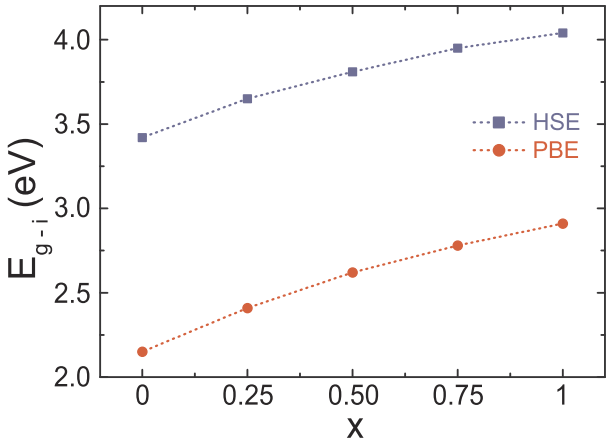

Fig. 6. The variation of band gap (E_{g-i}) of $Ga_{1-x}Al_xN$ with x. E_{g-i} calculated with PBE and HSE06 are shown by red and blue lines, respectively.

defined as:

$$E_g(Ga_{1-x}Al_xN) = xE_g(AlN) + (1-x)E_g(GaN) - \beta x(1-x) \quad (6)$$

and β is calculated as -0.35 eV. Albeit nonlinearity, evolution of band structure indicates that E_{g-i} can be adjusted continuously with varying x and thus tunable in the near UV range. In order to remove the possible constraints, the calculations at DFT-PBE level are repeated with 4×4 super cell and for different ordered configurations. Excluding the zone folding effects, similar electronic structure pattern is obtained and E_{g-i} only differs up to $\pm$ 0.1 eV which confirms that size does not alter the obtained results [26,55].

Finally, work function of alloys (Φ_w) which describes the photoelectric threshold of the material are calculated. Φ_w is a critical parameter to control the field-emission properties of 2D optoelectronic devices. Φ_w(GaN) and Φ_w(AlN) are calculated as 4.41 and eV 4.40 eV, respectively, which are compatible with the earlier results [62]. In parallel with the obtained results for pristine systems, Φ_w of alloys remains almost constant (~4.41 eV) and does not vary with the Al content.

3.5. Thermal properties

Following the analysis of the phonon modes, we calculate the heat capacity (C_v) of the $Ga_{1-x}Al_xN$ as the contribution of lattice vibrations mainly dominates C_v at all practical temperatures. C_v determines not only the thermal energy stored within the alloy but also how quickly it radiates heat. C_v at constant volume can be calculated by [52]:

$$C_v = \sum_{q_j} k_B \left(\frac{\hbar\omega_{q_j}}{k_B T}\right)^2 \frac{\exp(\hbar\omega_{q_j}/k_B T)}{[\exp(\hbar\omega_{q_j}/k_B T) - 1]^2} \quad (7)$$

where q is the wave vector, ω_{q_j} is the phonon frequency at q with phonon mode index j, T is the temperature, k_B is the Boltzmann constant and $\hbar$ is the reduced Planck constant. When compared, the variation of C_v(GaN) with T is compatible with earlier reports [63,64]. As expected, C_v increases with temperature for all compositions and converges to a constant value of 24 $J.K^{-1}.mol^{-1}$ as shown in Fig. 7 approaching Dulong-Petit limit. At low T (*i. e* up to 300 K), C_v gets smaller values with increasing x. It can be correlated with the shift of optical modes with increasing Al content (Fig. 3) as C_v varies much faster for high-frequency optical phonon modes than low-frequency acoustic phonon modes at low temperature [63].

3.6. Optical properties

The optical response of $Ga_{1-x}Al_xN$ is analyzed by calculating the imaginary part of dielectric function ($\epsilon_2(\omega)$) which is presented in Fig. 8. The absorption onsets of $Ga_{1-x}Al_xN$ blue-shift with increasing x

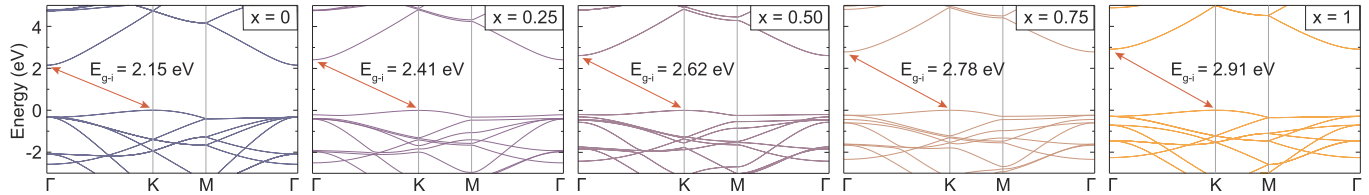

Fig. 5. The electronic band structures of $Ga_{1-x}Al_xN$ for x = 0, 0.25, 0.50, 0.75, 1. The 2×2 super cell (with respect to primitive unit cell of pristine system) is considered. The fundamental band gaps are shown by red arrows. Fermi level is set to zero.

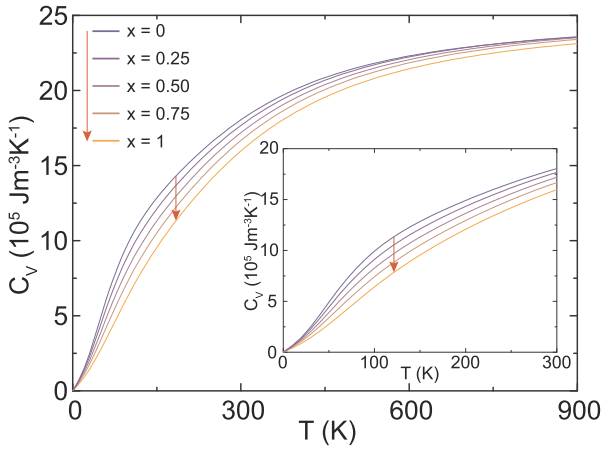

Fig. 7. The variation of heat capacity (C_v) of $Ga_{1-x}Al_xN$ with temperature for different values of x. Low temperature behavior (up to room temperature) of C_v is given as an inset.

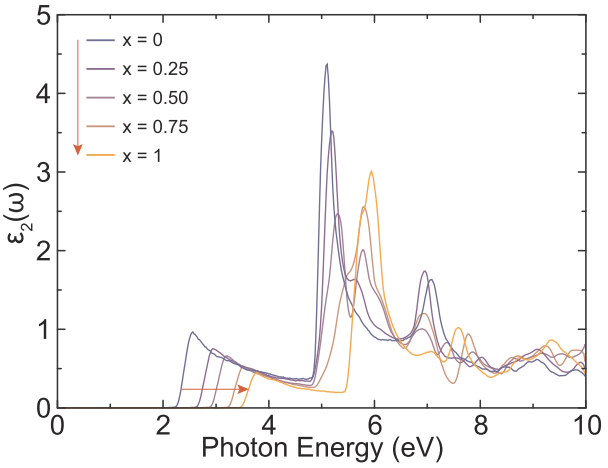

Fig. 8. The variation of imaginary dielectric function ($\epsilon_2(\omega)$) of $Ga_{1-x}Al_xN$ with photon energy for different values of x.

in compatible with the band gap of the structures. Main absorption peaks appear in the near UV region of the spectrum and they also shift to higher energy values as Al content increases. Moreover all systems have secondary remarkable absorption peak at far-UV region and their energies mainly depend on the constituent concentrations. The profile of $Ga_{0.75}Al_{0.25}N$ and $Ga_{0.25}Al_{0.75}N$ show similarity with the pristine h-GaN and h-AlN, respectively. While main peak of $Ga_{0.75}Al_{0.25}N$ ($Ga_{0.25}Al_{0.75}N$) blue-shifts, secondary absorption peak red-shifts when compared to h-GaN (h-AlN). In the case of $Ga_{0.5}Al_{0.5}N$ where Ga and Al contents are equal, two successive peaks for the main and secondary absorption are noticed indicating that the alloy possesses the character of both pristine systems equally. Due to the featured optical absorption over the UV range, alloys can be evaluated as a promising material for optoelectronic devices.

4. Conclusion

In summary, we design monolayer $Ga_{1-x}Al_xN$ ordered alloys with hexagonal lattice and investigate the variation of their structural, mechanical, electronic, thermal, and optical properties with concentration. We find that similar to pristine h-GaN and h-AlN, the planar geometry and hexagonal lattice are preserved. The optimized lattice constant gradually decreases with increasing x in accordance with Vegard's Law. The activation barrier to substitute Ga with Al is calculated to be low (79 meV) and moreover substitution is found to be energetically favorable. The mixing energy at ambient temperature is negative for all cases indicating that alloying is preferred against segregation. The phonon spectrum analysis and high temperature MD calculations further support the dynamical stability of the considered structures. The calculated in-plane stiffness indicates that $Ga_{1-x}Al_xN$ is softer than h-BN (or graphene) but has significantly high Poisson's ratio which is larger than most of the realized 2D systems. Similar to their pristine constituents, $Ga_{1-x}Al_xN$ alloys are wide, indirect band gap semiconductors. Band gap widens with increasing x, albeit the variation is not linear. Heat capacity of the alloys has a tendency to decrease with increasing Al content at low temperatures but approaches the classical limit at high temperatures. The absorption onset of the considered systems remain in the near UV range and prominent absorption peaks blue-shifts with increasing x in compliance with the variation of the band gap. The stability of $Ga_{1-x}Al_xN$ ordered alloys and their continuously tunable fundamental properties suggest these systems as promising 2D semiconductors for wide range of applications at reduced scales.

Acknowledgements

The calculations were performed at TUBITAK ULAKBIM, High Performance and Grid Computing Center (TR-Grid e-Infrastructure) and the National Center for High Performance Computing of Turkey (UHeM) under Grant No. 5003622015. This work was supported by the Scientific and Technological Research Council of Turkey (TUBITAK) under Project No 117F241. E.D. acknowledges support from The Turkish Academy of Sciences Outstanding Young Scientists Award Program (TUBA-GEBIP). A. M. acknowledges the Ankara University for high performance computing facility thorough the AYP under Grand No. 17A0443001.

Appendix A. Supplementary data

Supplementary data associated with this article can be found, in the online version, at https://doi.org/10.1016/j.commatsci.2019.05.018.

References

[1] C.R. Eddy Jr., N. Nepal, J.K. Hite, M.A. Mastro, J. Vac. Sci. Technol. A 31 (2013) 058501.
[2] H. Morkoc, Nitride Semiconductors and Devices 32 Springer Science & Business Media, 2013.
[3] S. Nakamura, Rev. Mod. Phys. 87 (2015) 1139.
[4] S. Mokkapati, C. Jagadish, Mater. Today 12 (2009) 22.
[5] P. Waltereit, O. Brandt, A. Trampert, H. Grahn, J. Menniger, M. Ramsteiner, M. Reiche, K. Ploog, Nature 406 (2000) 865.
[6] E. Durgun, S. Tongay, S. Ciraci, Phys. Rev. B 72 (2005) 075420.
[7] H. Şahin, S. Cahangirov, M. Topsakal, E. Bekaroglu, E. Akturk, R.T. Senger, S. Ciraci, Phys. Rev. B 80 (2009) 155453.
[8] H.L. Zhuang, A.K. Singh, R.G. Hennig, Phys. Rev. B 87 (2013) 165415.
[9] Z.Y. Al Balushi, K. Wang, R.K. Ghosh, R.A. Vilá, S.M. Eichfeld, J.D. Caldwell, X. Qin, Y.-C. Lin, P.A. DeSario, G. Stone, et al., Nat. Mater. 15 (2016) 1166.
[10] P. Tsipas, S. Kassavetis, D. Tsoutsou, E. Xenogiannopoulou, E. Golias, S. Giamini, C. Grazianetti, D. Chiappe, A. Molle, M. Fanciulli, et al., Appl. Phys. Lett. 103 (2013) 251605.
[11] V. Mansurov, T. Malin, Y. Galitsyn, K. Zhuravlev, J. Cryst. Growth 428 (2015) 93.
[12] D. Kecik, A. Onen, M. Konuk, E. Gürbüz, F. Ersan, S. Cahangirov, E. Aktürk, E. Durgun, S. Ciraci, Appl. Phys. Rev. 5 (2018) 011105.
[13] A. Onen, D. Kecik, E. Durgun, S. Ciraci, Phys. Rev. B 93 (2016) 085431.
[14] C. Bacaksiz, H. Sahin, H. Ozaydin, S. Horzum, R.T. Senger, F.M. Peeters, Phys. Rev. B 91 (2015) 085430.
[15] Y. Ma, Y. Dai, M. Guo, C. Niu, L. Yu, B. Huang, Appl. Surf. Sci. 257 (2011) 7845.
[16] M.S. Prete, A. Mosca Conte, P. Gori, F. Bechstedt, O. Pulci, Appl. Phys. Lett. 110 (2017) 012103.
[17] Y. Chen, J. Xi, D.O. Dumcenco, Z. Liu, K. Suenaga, D. Wang, Z. Shuai, Y.-S. Huang, L. Xie, ACS Nano 7 (2013) 4610.
[18] Q. Fang, Y. Huang, Y. Miao, K. Xu, Y. Li, F. Ma, J. Phys. Chem. C 121 (2017) 6605.
[19] A. Onen, D. Kecik, E. Durgun, S. Ciraci, Phys. Rev. B 95 (2017) 155435.
[20] A. Onen, D. Kecik, E. Durgun, S. Ciraci, J. Phys. Chem. C 121 (2017) 27098.
[21] Y. Mu, J. Phys. Chem. C 119 (2015) 20911.
[22] F. Ersan, A. Akcay, G. Gökoğlu, E. Aktürk, Chem. Phys. 455 (2015) 73.

[23] C. Schnohr, Appl. Phys. Rev. 2 (2015) 031304.
[24] W. Pfeiler, Alloy Physics: A Comprehensive Reference, John Wiley & Sons, 2008.
[25] S. Jain, M. Willander, J. Narayan, R.V. Overstraeten, J. Appl. Phys. 87 (2000) 965.
[26] V. Wang, Z. Wu, Y. Kawazoe, W.-T. Geng, J. Phys. Chem. C 122 (2018) 6930.
[27] J. Kang, S. Tongay, J. Li, J. Wu, J. Appl. Phys. 113 (2013) 143703.
[28] S. Tongay, D.S. Narang, J. Kang, W. Fan, C. Ko, A.V. Luce, K.X. Wang, J. Suh, K. Patel, V. Pathak, et al., Appl. Phys. Lett. 104 (2014) 012101.
[29] M. Zhang, J. Wu, Y. Zhu, D.O. Dumcenco, J. Hong, N. Mao, S. Deng, Y. Chen, Y. Yang, C. Jin, et al., ACS Nano 8 (2014) 7130.
[30] H. Li, X. Duan, X. Wu, X. Zhuang, H. Zhou, Q. Zhang, X. Zhu, W. Hu, P. Ren, P. Guo, et al., J. Am. Chem. Soc. 136 (2014) 3756.
[31] H.-P. Komsa, A.V. Krasheninnikov, J. Phys. Chem. Lett. 3 (2012) 3652.
[32] J. Lu, K. Zhang, X.F. Liu, H. Zhang, T.C. Sum, A.H.C. Neto, K.P. Loh, Nat. Commun. 4 (2013) 2681.
[33] I. Guilhon, L. Teles, M. Marques, R. Pela, F. Bechstedt, Phys. Rev. B 92 (2015) 075435.
[34] W.-X. Ji, C.-W. Zhang, M. Ding, P. Li, P.-J. Wang, J. Mater. Chem. C 5 (2017) 2649.
[35] J. Simon, V. Protasenko, C. Lian, H. Xing, D. Jena, Science 327 (2010) 60.
[36] L.-C. Duda, C.B. Stagarescu, J. Downes, K.E. Smith, D. Korakakis, T.D. Moustakas, J. Guo, J. Nordgren, Phys. Rev. B 58 (1998) 1928.
[37] L.-C. Xu, R.-Z. Wang, H. Yan, J. Phys. Chem. C 116 (2011) 1282.
[38] C. Pashartis, O. Rubel, Phys. Rev. B 96 (2017) 155209.
[39] M. Pandey, K.W. Jacobsen, K.S. Thygesen, J. Phys. Chem. C 120 (2016) 23024.
[40] T.L. Tan, M.-F. Ng, G. Eda, J. Phys. Chem. C 120 (2016) 2501.
[41] G. Kresse, J. Hafner, Phys. Rev. B 47 (1993) 558.
[42] G. Kresse, J. Hafner, Phys. Rev. B 49 (1994) 14251.
[43] G. Kresse, J. Furthmüller, Comput. Mater. Sci. 6 (1996) 15.
[44] G. Kresse, J. Furthmüller, Phys. Rev. B 54 (1996) 11169.
[45] P.E. Blöchl, Phys. Rev. B 50 (1994) 17953.
[46] G. Kresse, D. Joubert, Phys. Rev. B 59 (1999) 1758.
[47] J.P. Perdew, K. Burke, M. Ernzerhof, Phys. Rev. Lett. 77 (1996) 3865.
[48] H.J. Monkhorst, J.D. Pack, Phys. Rev. B 13 (1976) 5188.
[49] N.G. Limas, T.A. Manz, RSC Adv. 6 (2016) 45727.
[50] J. Heyd, G.E. Scuseria, M. Ernzerhof, J. Chem. Phys. 118 (2003) 8207.
[51] A.V. Krukau, O.A. Vydrov, A.F. Izmaylov, G.E. Scuseria, J. Chem. Phys. 125 (2006) 224106.
[52] A. Togo, I. Tanaka, Scr. Mater. 108 (2015) 1.
[53] L. Vegard, Z. Phys. 5 (1921) 17.
[54] A.R. Denton, N.W. Ashcroft, Phys. Rev. A 43 (1991) 3161.
[55] The calculated properties of ordered alloys are similar to the weighted averages, and obtained trends are expected to be valid for more realistic systems with random (disordered) configurations.
[56] H. Jónsson, G. Mills, K.W. Jacobsen, Classical and Quantum Dynamics in Condensed Phase Simulations, World Scientific, 1998, pp. 385–404.
[57] See Supplemental Material for Nudge Elastic Band and Molecular Dynamics results.
[58] R. Roldán, A. Castellanos-Gomez, E. Cappelluti, F. Guinea, J. Phys.: Condens. Matter 27 (2015) 313201.
[59] D. Akinwande, C.J. Brennan, J.S. Bunch, P. Egberts, J.R. Felts, H. Gao, R. Huang, J.-S. Kim, T. Li, Y. Li, et al., Extreme Mech. Lett. 13 (2017) 42.
[60] Z. Xu, Y. Li, Z. Liu, RSC Adv. 6 (2016) 113903.
[61] A. Falin, Q. Cai, E.J. Santos, D. Scullion, D. Qian, R. Zhang, Z. Yang, S. Huang, K. Watanabe, T. Taniguchi, et al., Nat. Commun. 8 (2017) 15815.
[62] Y. Mogulkoc, M. Modarresi, A. Mogulkoc, B. Alkan, Phys. Chem. Chem. Phys. 20 (2018) 12053.
[63] G. Qin, Z. Qin, H. Wang, M. Hu, Phys. Rev. B 95 (2017) 195416.
[64] Y. Jiang, S. Cai, Y. Tao, Z. Wei, K. Bi, Y. Chen, Comput. Mater. Sci. 138 (2017) 419.